IUST
Iran University of Science and Technology

Iranian Journal of Electrical and Electronic Engineering

Journal Homepage: ijeee.iust.ac.ir

Research Paper

Direct Power Control With NSTSM Algorithm for DFIG Using SVPWM Technique

H. Benbouhenni*(C.A.), Z. Boudjema**, A. Belaidi*

Abstract: The paper presents a super-twisting sliding mode (STSM) regulator with neural networks (NN) of direct power command (DPC) for controlling the active/reactive power of a doubly-fed induction generator (DFIG) using a two-level space vector pulse width modulation (2L-SVPWM). Traditional DPC strategy with proportional-integral (PI) controllers (DPC-PI) has significantly more active/reactive power ripples, electromagnetic torque ripple, and harmonic distortion (THD) of voltages. The proposed DPC strategy based on a neural super-twisting sliding mode controller (NSTSM) minimizes the THD of stator/rotor voltage, reactive/active power ripple, rotor/stator current, and torque ripples. Also, the DPC method with NSTSM controllers (DPC-NSTSM) is a simple algorithm compared to the vector control method. Both methods are developed and programmed in Matlab on a 1.5MW DFIG-based wind turbines. The simulation studies of the DPC technique with the NSTM algorithm have been performed, and the results of these studies are presented and discussed.

Keywords: STSM, NN, DPC, PI, DFIG, NSTSM, 2L-SVPWM, DPC-NSTSM, THD, DPC-PI.

1 Introduction

DOUBLY fed induction generator (DFIG) is one of the most generators for generating electric energy [1]. The control of this machine has recently become a major concern for researchers [2]. The DFIG is fed by two converters, one of them is from the generator side and it is called RSC, and the other side of the electrical network is called GSC [3]. The advantages of the DFIG is detailed in [1]. So, various methods have been proposed for DFIGs. In [4], a direct vector control (DVC) has proposed, which based on fuzzy space vector modulation to command DFIG-based WTSs. Indirect vector command (IVC) is designed to command the rotor flux/torque of DFIG integrated to wind turbines (WTs) [5]. Direct torque control (DTC) was designed to command the torque and rotor flux of DFIG [6]. In this strategy method, one switching table and two hysteresis comparators of flux and torque to control the inverter [7]. In [8], the DTC method was proposed based on the second-order continuous sliding mode (SOCSM) algorithm. DTC and neural algorithms are combined to regulate the torque of DFIG [9]. Backstepping control of wind turbine was designed to control rotor flux and torque [10]. Similar to the conventional DTC method, a DPC (Direct Power Control) strategy of DFIG-WT has proposed recently [11-13]. However, DPC control offers many advantages: simplicity in calculations, fast dynamic response, and robustness against machine parameter mismatches. In [14], the DPC method based on an estimated stator flux (ESF) has been proposed. In [15], a new DPC method was designed based on a stator flux oriented (SFO) command with a constant switching frequency. In this proposed DPC method, the reference rotor voltage was calculated based on the ESF method, reactive and active powers, and their errors. DPC and SOCSMC techniques are combined to command DFIG-

Iranian Journal of Electrical and Electronic Engineering, 2021.
Paper first received 05 June 2019, revised 09 June 2020, and accepted 16 June 2020.
* The authors are with the Laboratoire d'Automatique et d'Analyse des Systèmes (LAAS), Departement de Génie Électrique, Ecole Nationale Polytechnique d'Oran Maurice Audin, Oran, Algeria.
E-mails: habib0264@gmail.com and belaidiaek@gmail.com.
** The author is with the Laboratoire Génie Électrique ET Energies Renouvelables (LGEER), Electrical Engineering Department, Hassiba Benbouali University, Chlef, Algeria.
E-mail: boudjemaa1983@yahoo.fr.
Corresponding Author: H. Benbouhenni.
https://doi.org/10.22068/IJEEE.17.1.1518

WT [16]. In [17], an improved DPC control scheme of a DFIG-WTs connected to an electrical network was presented. In [18], DPC control based on fuzzy logic has been proposed. This controller provides advantages such as reduced the torque ripples and THD value of voltage. In [19], DPC is presented based on the DSVM method (discrete space vector modulation), and fuzzy logic is used to reduce power ripples. The twelve sectors DPC based on neural hysteresis comparators was presented [20]. In [21], a neural networks based DPC strategy (NDPC) is proposed for DFIG-based WECS by using neural pulse width modulation technique (NPWM). In [22], a DPC technique based on the SVPWM strategy (space vector pulse width modulation) is designed to command the power and torque of DFIG-WT. In [23], the author proposes a new DPC control scheme using a neural switching table of DFIG-WECS. DPC and neural SVPWM technique are combined to control the permanent magnet synchronous generator (PMSG) [24]. In [25], the DPC strategy based on a three-level neural SVPWM technique has been proposed. This proposed technique reduced the torque/flux ripple compared to the classical DPC method of the DFIG-WT. A five-level DPC technique based on a neural network algorithm is proposed to regulate the torque/power of the DFIG-WT [26]. Seven-level SVPWM technique is designed to command the torque and rotor flux/power of the DFIG-WT controlled by the DPC strategy [27]. In [28], the author proposes a new DTC control scheme based on the fuzzy STSM algorithm (FSTSM) to minimizes the harmonic distortion of stator current for DFIG-based wind turbine.

In this work, a new direct power control technique for DFIG in WT systems is proposed. The proposed technique is DPC control with a neural super-twisting sliding mode controller (DPC-NSTSMC). The proposed control technique preserves the advantages of the traditional DPC control such as fast response, fewer parameters dependence and simplicity. On the other hand, the proposed method minimized the THD value of voltage/current, flux/torque ripple and active/reactive power ripple compared to conventional DPC, and DPC-PI method. The stability of the NSTSM is proven using the Lyapunov technique. Finally, the proposed, and traditional DPC-PI methods performance is verified by the simulation study on the DFIG system under reference tracking and THD of stator current.

2 DFIG Modeling

The mathematical model implementation of DFIG in the synchronous reference frame is [29, 30]:

$$\begin{cases} \psi_{ds} = L_s I_{ds} + M I_{dr} \\ \psi_{qs} = L_s I_{qs} + M I_{qr} \\ \psi_{dr} = L_r I_{dr} + M I_{ds} \\ \psi_{qr} = L_r I_{qr} + M I_{qs} \end{cases} \quad (1)$$

where, L_r is the inductance of the rotor, Ψ_{dr} and Ψ_{qr} is the rotor fluxes, M is the mutual inductance, L_s is the inductance of the stator, Ψ_{qs} and Ψ_{ds} is the stator fluxes.

$$\begin{cases} V_{ds} = R_s I_{ds} + \dfrac{d}{dt}\psi_{ds} - \omega_s \psi_{qs} \\ V_{qs} = R_s I_{qs} + \dfrac{d}{dt}\psi_{qs} + \omega_s \psi_{ds} \\ V_{dr} = R_r I_{dr} + \dfrac{d}{dt}\psi_{dr} - \omega_r \psi_{qr} \\ V_{qr} = R_r I_{qr} + \dfrac{d}{dt}\psi_{qr} + \omega_r \psi_{dr} \end{cases} \quad (2)$$

where, I_{dr} and I_{qr} are the rotor currents, V_{ds} and V_{qs} are the stator voltages, I_{ds} and I_{qs} are the stator currents, R_r is the rotor resistance, V_{dr} and V_{qr} are the rotor voltages, R_s is the stator resistance, wr.

The mechanical equation of the DFIG is given by the following equation:

$$T_{em} = T_r + J \cdot \frac{d\Omega}{dt} + f \cdot \Omega \quad (3)$$

where, T_e is the electromagnetic torque, Ω is the mechanical rotor speed, T_r is the load torque, f is the viscous friction coefficient, J is the inertia.

The torque T_e can be written as follows:

$$T_{em} = \frac{3}{2}.p.\frac{M}{L_s}(\psi_{qs}.I_{dr} - \psi_{ds}.I_{qr}) \quad (4)$$

The reactive and active powers of the DFIG is given by the following relationships as:

$$\begin{cases} P_s = \dfrac{3}{2}(V_{ds} I_{ds} + V_{qs} I_{qs}) \\ Q_s = \dfrac{3}{2}(V_{qs} I_{ds} - V_{ds} I_{qs}) \end{cases} \quad (5)$$

where, Q_s is the stator reactive power, P_s is the stator active power.

3 DPC-PI Control Scheme

The DPC with PI controllers is used to command the DFIG power/torque magnitude. Q_s are controlled by direct-axis voltage (V_{dr}), and P_s are controlled by quadrature-axis voltage (V_{qr}). This command method is a simple algorithm and gives a fast response dynamic [31].

The major problem of the DPC-PI control scheme is the power ripples and THD value of stator voltage. The proposed DPC-PI method designed to command the active/reactive power of the DFIG-WT is illustrated in Fig. 1.

The rotor flux is estimated by using (6):

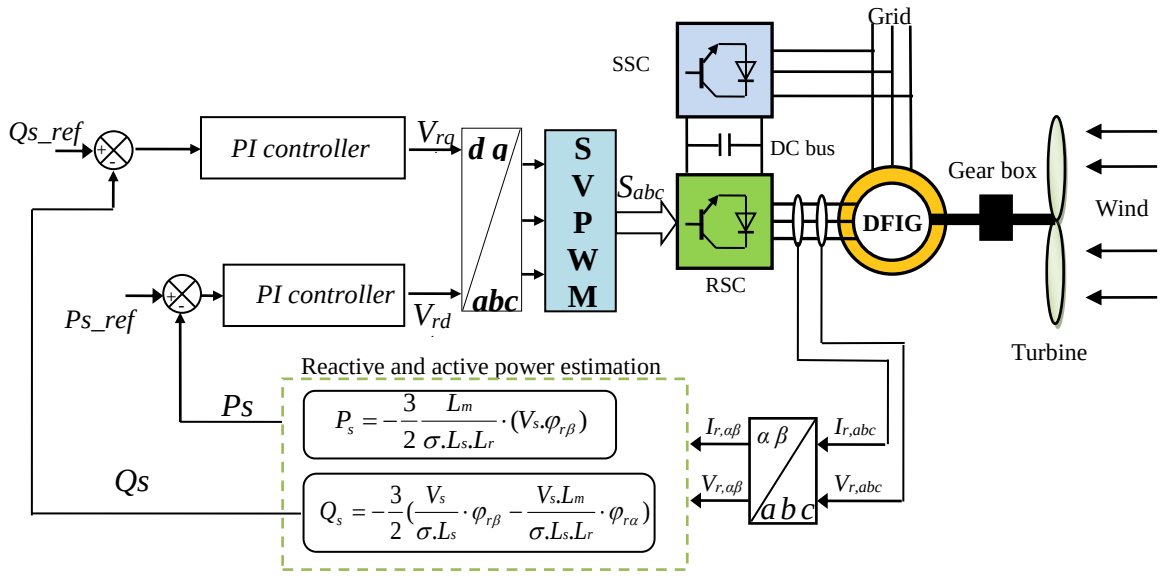

Fig. 1 Schematic diagram of DPC-PI strategy for DFIG.

$$\begin{cases} \Psi_{r\alpha} = \int_0^t (V_{r\alpha} - R_r I_{r\alpha}) dt \\ \Psi_{r\beta} = \int_0^t (V_{r\beta} - R_r I_{r\beta}) dt \end{cases} \quad (6)$$

where, $V_{r\alpha}$ is the rotor voltage linkage (RVL) of α-axis, $V_{r\beta}$ is the RVL of β-axis.

The stator flux is given by:

$$\Psi_s = \sqrt{\Psi_{s\alpha}^2 + \Psi_{s\beta}^2} \quad (7)$$

where, Ψ_s is the stator flux.

The angle stator flux is given by:

$$\theta_s = \text{arctg}\left(\frac{\Psi_{s\beta}}{\Psi_{s\alpha}}\right) \quad (8)$$

Active and reactive powers is estimated using (9) and (10) [32].

$$P_s = -\frac{3}{2}\frac{L_m}{\sigma . L_s . L_r} \cdot (V_s . \phi_{r\beta}) \quad (9)$$

$$Q_s = -\frac{3}{2}\left(\frac{V_s}{\sigma . L_s} \cdot \phi_{r\beta} - \frac{V_s . L_m}{\sigma . L_s . L_r} \cdot \phi_{r\alpha}\right) \quad (10)$$

where, L_m is the mutual inductance, $\Psi_{r\beta}$ is the RFL of β-axis, $\Psi_{r\alpha}$ is the RFL of α-axis, and

$$\sigma = 1 - \frac{M^2}{L_r L_s} \quad (11)$$

$$\Psi_{s\alpha} = \sigma L_r I_{r\alpha} + \frac{M}{L_s}\Psi_s \quad (12)$$

where, $\Psi_{s\alpha}$ is the stator flux linkage of α-axis, $I_{r\alpha}$ is the rotor current linkage of α-axis.

$$\Psi_{s\beta} = \sigma L_r I_{r\beta} \quad (13)$$

where $\Psi_{s\beta}$ is the stator flux linkage (SFL) of β-axis and $I_{r\beta}$ is the RCL of β-axis.

$$\left|\overline{V_s}\right| = \left|\overline{\Psi_s}\right| w_s \quad (14)$$

where, V_s is the stator voltage.

The active/reactive power can be reformulated by inducing angle λ between the stator and rotor vectors as follows:

$$P_s = -\frac{3}{2}\frac{L_m}{\sigma . L_s . L_r} w_s |\psi_s||\psi_r| \sin(\lambda) \quad (15)$$

$$Q_s = -\frac{3}{2}\frac{w_s}{\sigma . L_s}|\psi_s|\left(\frac{M}{L_r}|\psi_r|\cos(\lambda) - |\psi_s|\right) \quad (16)$$

The derivation of the reactive/active power of the DFIG can be given by:

$$\frac{dP_s}{dt} = -\frac{3}{2}\frac{L_m}{\sigma . L_s . L_r} w_s |\psi_s| \frac{d(|\psi_r| \sin(\lambda))}{dt} \quad (17)$$

$$\frac{dQ_s}{dt} = -\frac{3}{2}\frac{M w_s}{\sigma . L_r L_s}|\psi_s| \frac{d(|\psi_r| \cos(\lambda))}{dt} \quad (18)$$

4 DPC Control With NSTSMC Controller

To improve the DPC-PI method, complimentary use of the neural STSM algorithm (NSTSM) is proposed. The principle of the DPC-NSTSM method is similar to the DPC-PI strategy. The difference is using an NSTSM algorithm to replace the PI controllers. As shown in Fig. 2.

On the other hand, the proposed method is a simple algorithm compared to the vector control strategy. This method reduces the reactive and active powers ripples.

The STSM active and reactive power regulators are designed to respectively change the q and d-axis voltages as in (19) and (20) [33, 34].

$$\begin{cases} V_{dr} = K_1 \left| S_{Q_s} \right|^r \operatorname{sgn}(S_{Q_s}) + \dot{V}_{dr1} \\ \dot{V}_{dr1} = K_2 \operatorname{sgn}(S_{Q_s}) \end{cases} \tag{19}$$

$$\begin{cases} V_{qr} = K_1 \left| S_{P_s} \right|^r \operatorname{sgn}(S_{P_s}) + \dot{V}_{qr1} \\ \dot{V}_{dr1} = K_2 \operatorname{sgn}(S_{P_s}) \end{cases} \tag{20}$$

where the stator reactive power magnitude error $S_{Qs} = Q_{sref} - Q_s$ and the stator active power error $S_{Ps} = P_{sref} - P_s$ are the sliding variables, and the constant gains k_1 and k_2 must check the stability conditions.

Fig. 3 shows the block diagram of STSMC control strategy.

Consider a dynamic system with input u, output y and state x, given by (21).

$$\frac{dx}{dt} = a(x,t) + b(x,t)u, \quad y = c(x,t) \tag{21}$$

The command difficulty is to discover an input

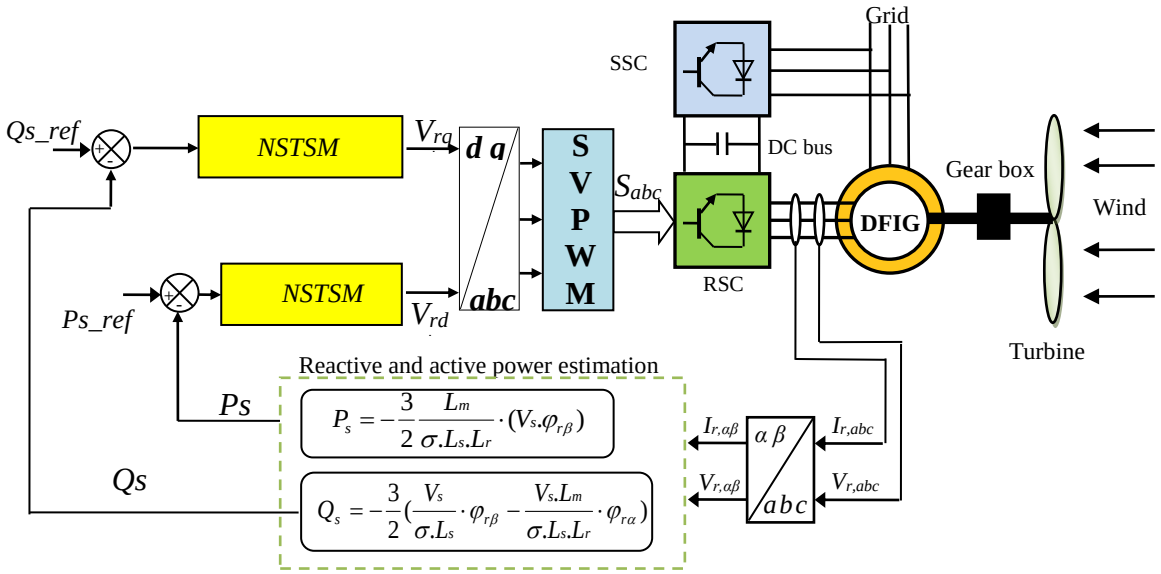

Fig. 2 Schematic diagram of DPC-NSTSMC for DFIG.

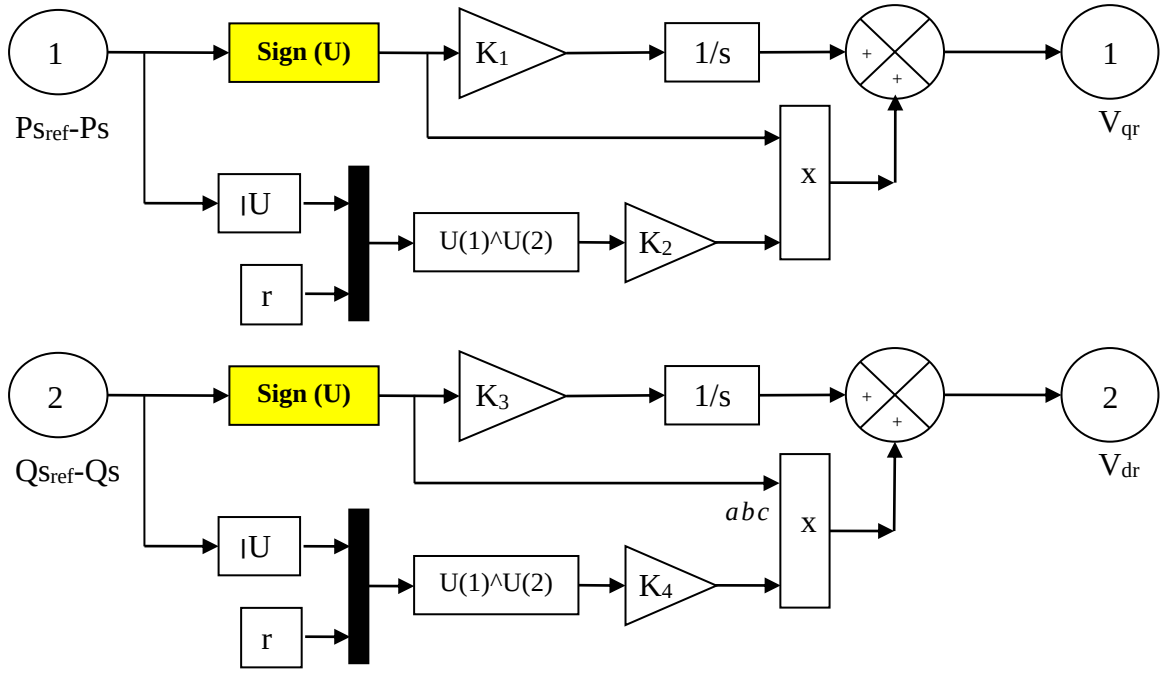

Fig. 3 Block diagram of STSMC technique.

function $u = f(y, \dot{y})$ which can drives the system trajectories to the starting point y = $\dot{y}$ = 0 of the phase plane, if possible in limited time. The input u is defined as a novel state variable, where as the switching command is applied to its time derivative, $\dot{u}_1$.

The output y is controlled by a STSMC, with the sliding variable (SV) $S = y^* - y$.

This algorithm does not utilize the derivative of the SV. As imposed by (22), the adequate condition for convergence to the sliding surface and for stability is for the gains to be large enough [35].

$$u = K_1 |S|^r \operatorname{sgn}(S) + u_1$$
$$\dot{u}_1 = K_2 \operatorname{sgn}(S) \tag{22}$$

$$K_1 > \frac{A_M}{B_m}, \quad K_2 \geq \frac{4A_M}{B_m^2} \cdot \frac{B_M (K_1 + A_M)}{B_m (K_1 - A_M)} \tag{23}$$

where $A_M \geq |A|$ and $B_M \geq B \geq B_m$ are superior and inferior bounds of A and B in the second derivative of y.

$$\frac{d^2 y}{dt^2} = A(x,t) + B(x,t) \frac{du}{dt} \tag{24}$$

The NSTSMC is similar to a traditional STSMC controller. On the other hand, the switching controller term has been replaced by the neural algorithm as shown by Fig. 4. The NSTSMC reduce the THD value of current/voltage, active/reactive power ripples compared to the classical technique.

The structure of the proposed neural algorithms was a network with 8 neurons in the hidden layer, one linear input node, and one neuron in the output layers. Fig. 5 shows the block diagram of the ANN controller for reactive/active power. Fig. 6 show the block diagram of the hidden layer.

Fig. 7 shows the neural algorithm training performance of ANN controllers for switching controllers.

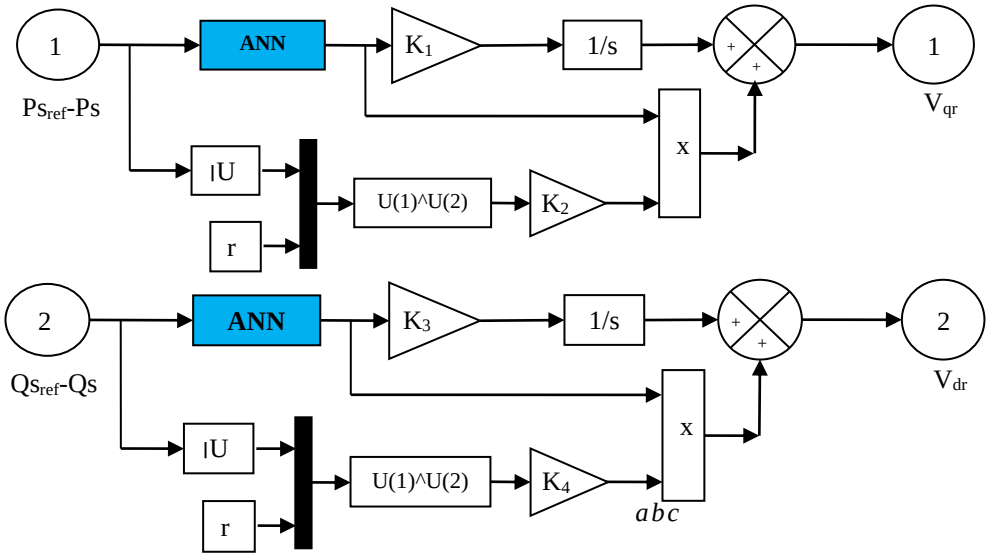

Fig. 4 Block diagram of NSTSMC strategy.

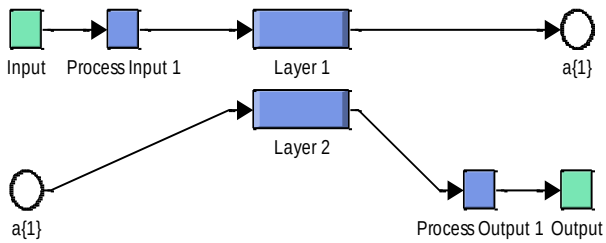

Fig. 5 The internal structure of ANN controller.

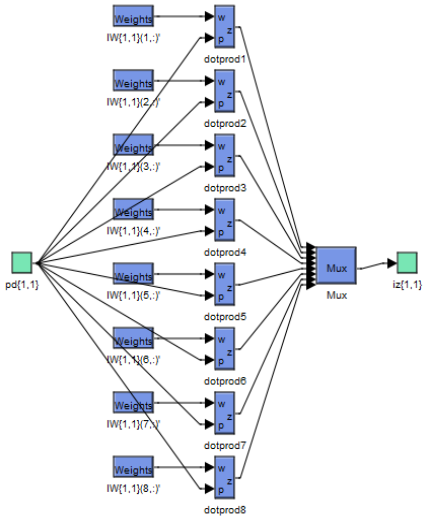

Fig. 6 Hidden layer.

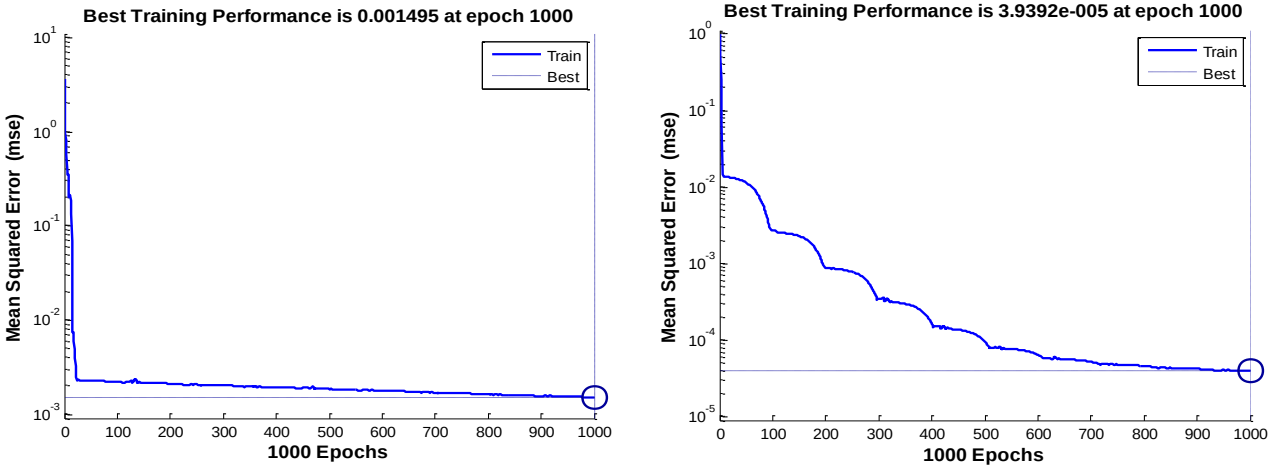

Fig. 7 The internal structure of ANN controller; a) a) Active power and b) Reactive power.

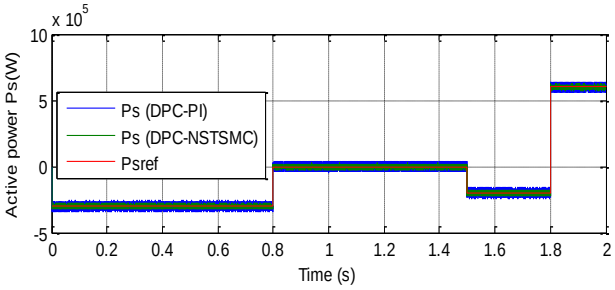

Fig. 8 Active power (RTT).

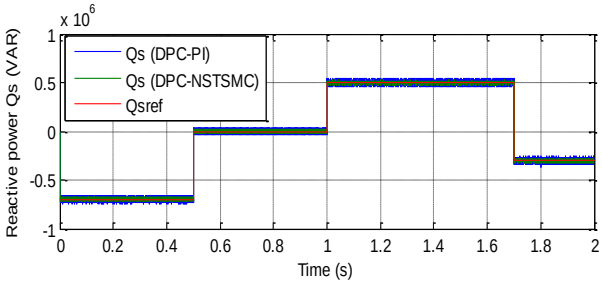

Fig. 9 Reactive power (RTT).

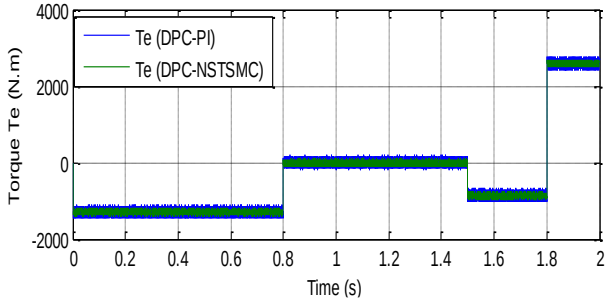

Fig. 10 Electromagnetic torque (RTT).

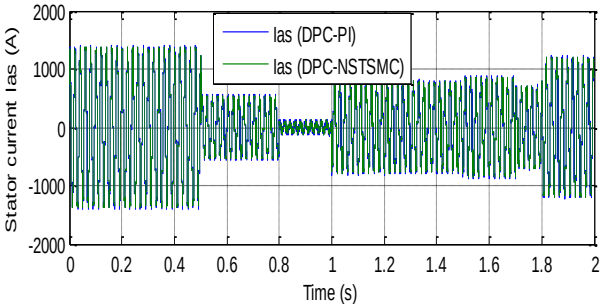

Fig. 11 Stator current (RTT).

5 Results

The simulation results of DPC with the NSTSMC controller of a 1.5 MW DFIG are compared with the DPC-PI method. The two control strategies were compared, using two tests to find out which control was better than the other. The performance analysis is done with electromagnetic torque, harmonic distortion of current, reactive and active powers. DFIG used for the simulations has the following parameters: P_n = 1.5 MW, V_n = 398 V, f = 50 Hz, R_s = 0.012 Ω, M = 0.0135 H, L_s = 0.0137 H, R_r = 0.021 Ω, L_r = 0.0136 H, J = 1000 Kg.m^2, f_r = 0.0024 Nm/s [36].

5.1 Reference Tracking Test (RTT)

Table 1 presents the THD of the proposed control strategies. it is apparent that the THD value of current for the DPC-NSTSMC method is considerably reduced (see Figs. 12 and 13).

Table 1 The THD (RTT).

	THD [%]	
	DPC-PI	DPC-NSTSMC
Stator current	2.19	1.26

For the DPC-PI and DPC-NSTSMC control scheme, the stator reactive power (Q_s) and active power (P_s) tracks almost perfectly their reference values (P_{sref} and Q_{sref}) (See Figs. 8 and 9). The active and reactive powers are decoupled from each other in the DPC-NSTSMC control with a rapid time response, without overshoot, and with a minimal static error. Fig. 10 shows the torque of the DPC-PI and DPC-NSTSMC control scheme. Fig. 11 shows the current of the proposed control and DPC-PI control scheme. Stator

active power response comparing curves are shown in Fig. 14. See figure the stator active power ripples is significantly reduced when the DPC-NSTSMC control is in use. Fig. 15 shows the stator reactive power responses of both the DPC-PI and DPC-NSTSMC strategy. It is found that the DPC-NSTSMC control scheme exhibits smooth response and lesser ripple in reactive power as compared to the DPC-PI method. On the other hand, the DPC-NSTSMC method minimized the torque ripples compared to the DPC-PI strategy (See Fig. 16). Fig. 17 shows the zoom in the current of the DPC-NSTSMC and DPC-PI strategies. This figure shows that the ripples of stator current for the DPC-NSTSMC method has reduced compared to DPC-PI.

5.2 Robustness Test (RT)

In this section, the resistances R_s and R_r are multiplied by 2 and the values of the inductances L_s and L_r are divided by 2. Simulation results are presented in Figs. 18-23. As it is shown by these figures, these variations present a clear effect on reactive power, electromagnetic

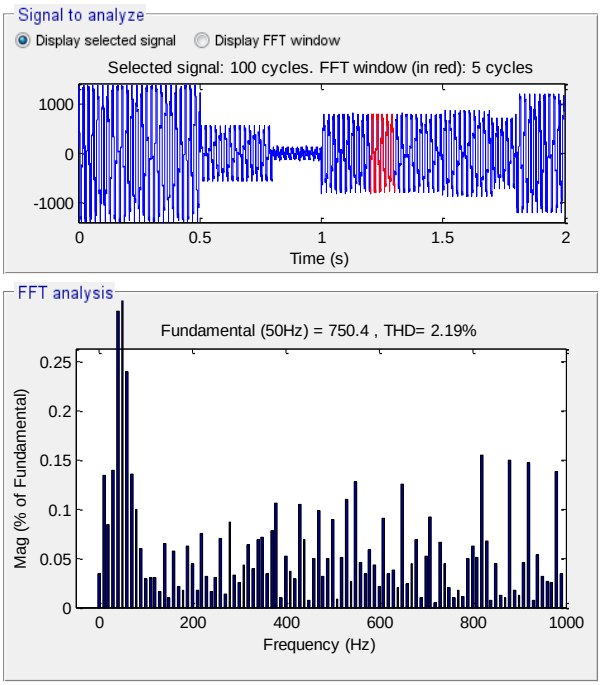

Fig. 12 THD of current I_{as} (DPC-PI).

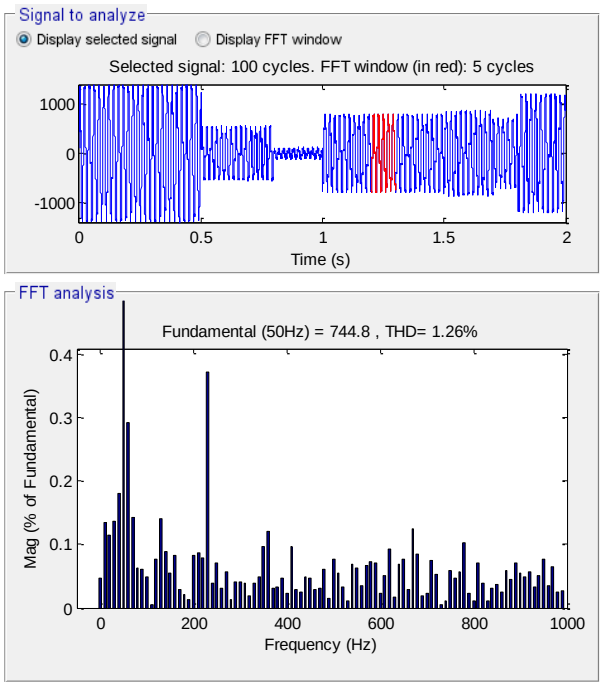

Fig. 13 THD of current I_{as} (DPC-NSTSMC).

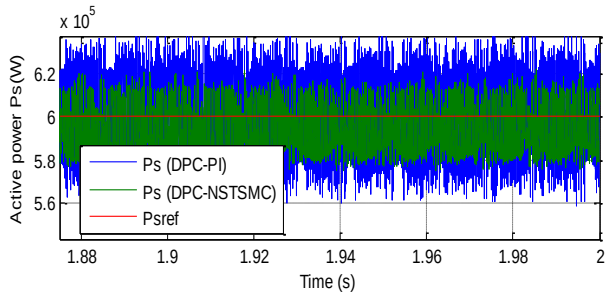

Fig. 14 Zoom in P_s (RTT).

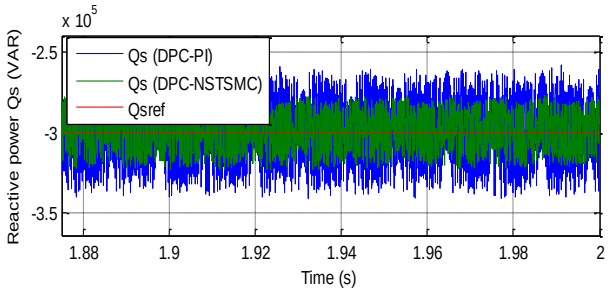

Fig. 15 Zoom in Q_s (RTT).

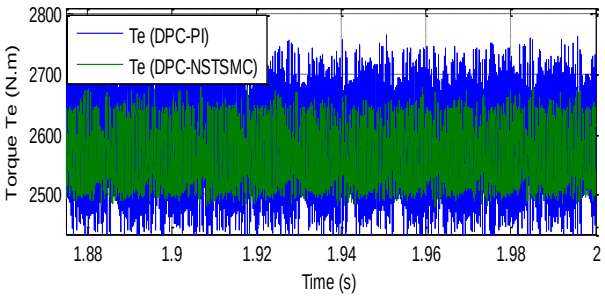

Fig. 16 Zoom in the electromagnetic torque (RTT).

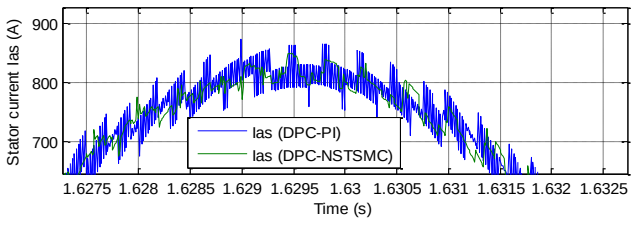

Fig. 17 Zoom in I_{as} (RTT).

torque, active power, and current curves and that the effect appears more important for the DPC-PI than that with DPC-NSTSMC control (see Figs. 24-27). In addition, these results show that the THD value of stator current in the DPC-NSTSMC method has been minimized significantly (see Figs. 18 and 19). Table 2 presents the THD values of both techniques. Thus, it can be concluded that the proposed DPC-NSTSMC method is more robust than the DPC-PI one.

Table 2 The THD (RT).

	THD [%]	
	DPC-PI	DPC-NSTSMC
I_{as} current	4.84	2.98

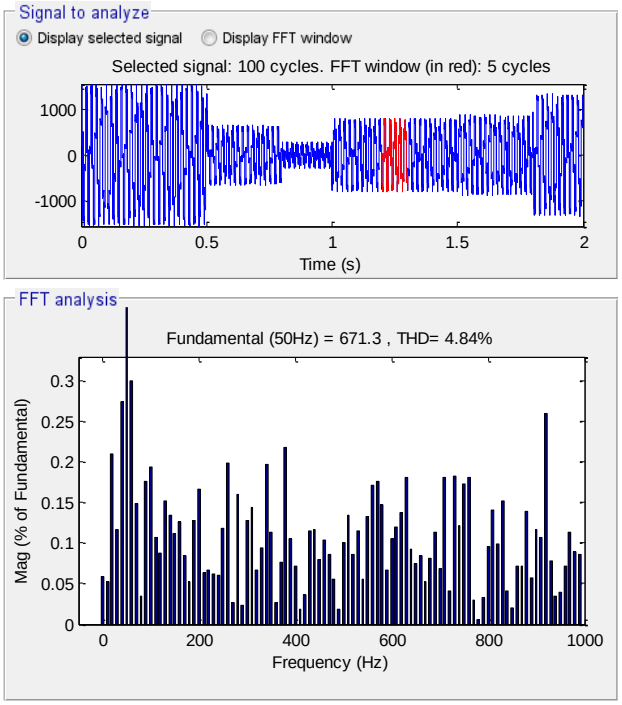

Fig. 18 The THD of current I_{as} (DPC-PI).

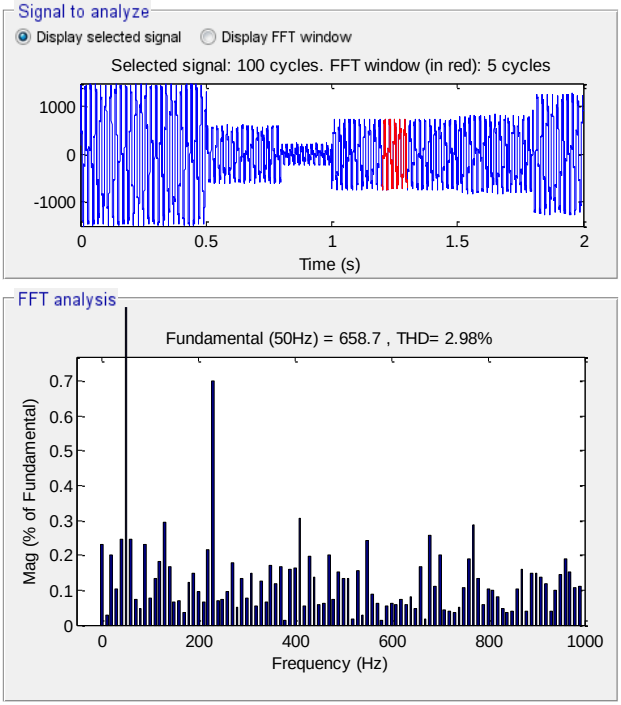

Fig. 19 The THD of current I_{as} (DPC-NSTSMC).

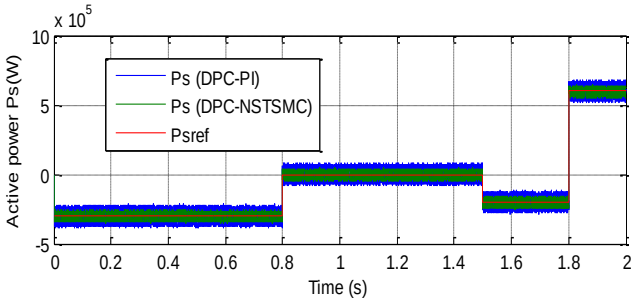

Fig. 20 Active power.

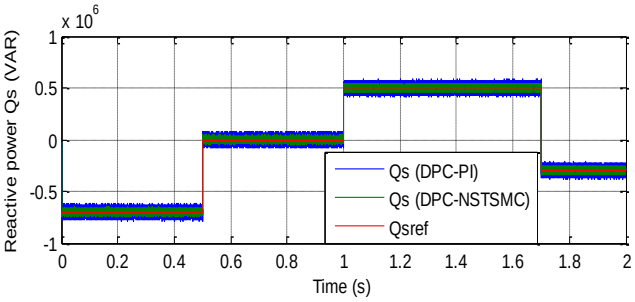

Fig. 21 Reactive power.

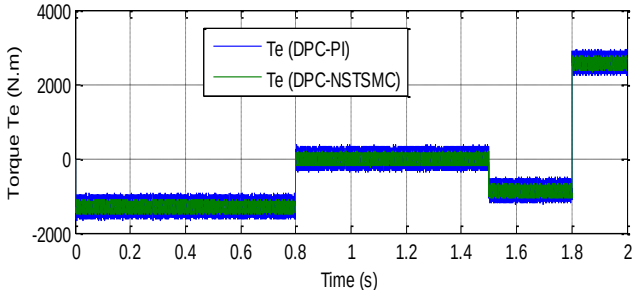

Fig. 22 Electromagnetic torque.

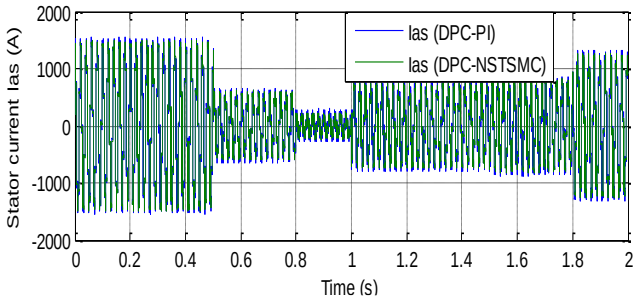

Fig. 23 I_{as} current (RT).

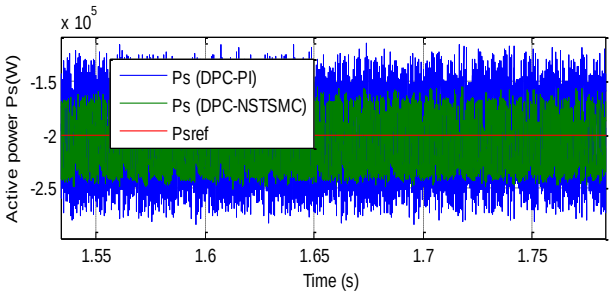

Fig. 24 Zoom in P_s (RT).

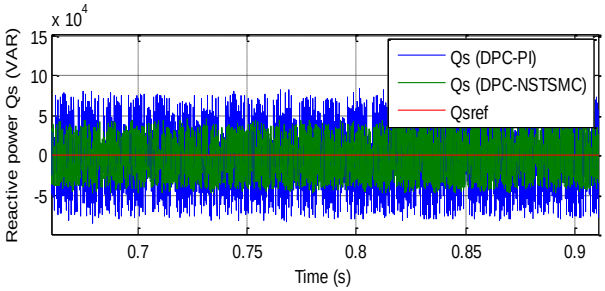

Fig. 25 Zoom in Q_s (RT).

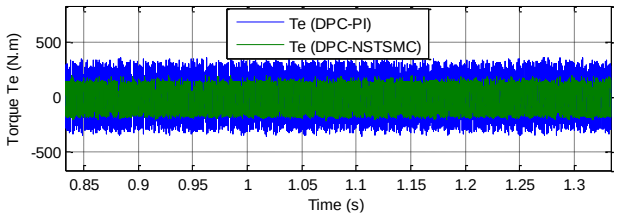

Fig. 26 Zoom in the torque (RT).

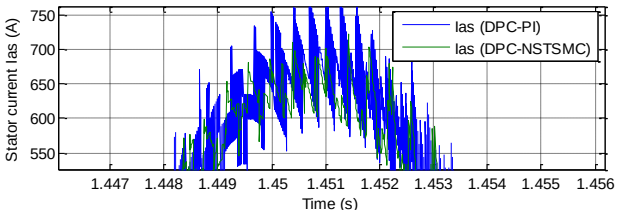

Fig. 27 Zoom in I_{as} (RT).

6 Conclusion

In this work, a new DPC algorithm based on neural network, super twisting sliding mode and SVPWM for a DFIG-based WTS are presented. A comparison of this method with a DPC-PI is elaborated by using different simulation tests. The results obtained showed the superiority of the proposed technique compared to DPC-PI. The performances brought by the proposed technique appeared especially in the reduction of the DFIG powers ripples while keeping the robustness of the control. These results can actively contribute to improving the conditions for connecting the DFIG-based wind system to the electricity grid.

Appendix

a) The Coefficients of the PI Reactive and Active Powers Regulators

Table 3 shows the constants values of the active/reactive power PI controllers gains (K_{ip}, K_{pp}, K_{iq}, and K_{pq}).

Table 3 PI regulator gaines.

P_s		Q_s	
K_i	K_p	K_p	K_i
1000	100	100	1000

b) The Coefficients of the NSTSM Reactive/Active Power Regulators

Table 4 shows the constants values of the reactive/active power NSTSM algorithm gains (K_1, K_2, K_3, and K_4).

Table 4 NSTSM algorithm gaines.

P_s			Q_s		
K_3	K_4	r	K_1	K_2	r
200	1000	0.5	200	1000	0.5

References

[1] Y. Wa and W. Yang, "Different control strategies on the rotor side converter in DFIG based wind turbines," *Energy Procedia*, Vol. 100, pp. 551–555, 2016.

[2] E. G. Shehata, "Sliding mode direct power control of RSC for DFIGs driven by variable speed wind turbines," *Alexandria Engineering Journal*, Vol. 54, pp. 1067–1075, 2015.

[3] H. Benbouhenni, Z. Boudjema, A. Belaidi, "DFIG-based WT system using FPWM inverter," *International Journal of Smart Grid*, Vol. 2, No. 3, pp. 142–154, 2018.

[4] H. Benbouhenni, Z. Boudjema, and A. Belaidi, "Intelligent SVM technique of a multi-level inverter for a DFIG-based wind turbine system," *International Journal of Digital Signals and Smart Systems*, Vol. 3, Nos. 1–3, pp.4–19, 2019.

[5] H. Benbouhenni, Z. Boudjema, and A. Belaidi, "Indirect vector control of a DFIG supplied by a two-level FSVM inverter for wind turbine system," *Majlesi Journal of Electrical Engineering*, Vol. 13, No. 1, pp. 45–54, 2019.

[6] S. Z. Chen, N. C. Cheung, K. C. Wong, and J. Wu, "Integral variable structure direct torque control of doubly fed induction generator," *IET Renewable Power Generation*, Vol. 5, No. 1, pp. 18–25, 2011.

[7] Z. Boudjema, R. Taleb, and A. Yahdou, "A new DTC scheme using second order sliding mode and fuzzy logic of a DFIG for wind turbine system," *International Journal of Advanced Science and Applications*, Vol. 7, No. 8, pp. 49–56, 2016.

[8] Z. Boudjema, R. Taleb, Y. Djerriri, A. Yahdou, "A novel direct torque control using second order continuous sliding mode of a doubly fed induction generator for a wind energy conversion system," *Turkish Journal of Electrical Engineering & Computer Sciences*, Vol. 25, pp. 965–975, 2017.

[9] A. Bakouri, H. Mahmoudi, and A. Abbou, "Intelligent control for doubly fed induction generator connected to the electrical network," *International Journal of Power Electronics and Drive System*, Vol. 7, No. 3, pp. 688–700, 2016.

[10] M. EL Azzaoui, H. Mahmoudi, and K. Boudaraia, "Backstepping control of wind and photovoltaic hybrid renewable energy system," *International Journal of Power Electronics and Drive System*, Vol. 7, No. 3, pp. 677–686, 2016.

[11] S. Jou, S. Lee, Y. Park, and K. Lee, "Direct power control of a DFIG in wind turbines to improve dynamic responses," *Journal of Power Electronics*, Vol. 9, No. 5, pp. 781–790, 2009.

[12] H. Nian, Y. Song, P. Zhou, and Y. He, "Improved direct power control of a wind turbine driven doubly fed induction generator during transient grid voltage unbalance," *IEEE Transactions on Energy Conversion*, Vol. 26, No. 3, pp. 976–985, 2011.

[13] G. Abad, M. A. Rodriguez, G. Iwanski, and J. Poza, "Direct power control of doubly-fed-induction-generator-based wind turbines under unbalanced grid voltage," *IEEE Transactions on Power Electronics*, Vol. 25, No. 2, 2010.

[14] L. Xu and P. Cartwright, "Direct active and reactive power control of DFIG for wind energy generation," *IEEE Transactions on Energy Conversion*, Vol. 21, No. 3, pp. 750–758, 2006.

[15] D. Zhi, L. Xu, "Direct power control of DFIG with constant switching frequency and improved transient performance," *IEEE Transactions on Energy Conversion*, Vol. 22, No. 1, pp. 110–118, 2007.

[16] A. Bouyekni, R. Taleb, Z. Boudjema, and H. Kahal, "A second-order continuous sliding mode based on DFIG for wind-turbine-driven DFIG," *Elektrotehniški Vestnik*, Vol. 85, No. 1-2, pp. 29–36, 2018.

[17] E. G. Shehata, M. Gerges, and M. Salama, "Direct power control of DFIGs based wind energy generation systems under distorted grid voltage conditions," *International Journal of Electrical Power & Energy Systems*, Vol. 53, pp. 956–966, 2013.

[18] M. V. Kazemi, M. Moradi, and R. V. Kazemi, "Minimization of powers ripple of direct power controlled DFIG by fuzzy controller and improved discrete space vector modulation," *Electric Power Systems Research*, Vol. 89, pp. 23–30, 2012.

[19] M. Pichan, H. Rastegar, and M. Monfared, "Two fuzzy-based direct power control strategies for doubly-fed induction generators in wind energy conversion systems," *Energy*, Vol. 51, pp. 154–162, 2013.

[20] H. Benbouhenni, "Twelve sectors DPC control based on neural hysteresis comparators of the DFIG integrated to wind power," *Tecnica Italiana-Italian Journal of Engineering Science*, Vol. 64, No. 2, pp. 223–236, 2020.

[21] H. Benbouhenni, Z. Boudjema, and A. Belaidi, "Power control of DFIG in WECS using DPC and NDPC-NPWM methods," *Mathematical Modelling of Engineering Problems*, Vol. 7, No. 2, pp. 223–236, 2020.

[22] S. Massoum, A. Meroufel, A. Massoum, and P. Wira, "A direct power control of the doubly-fed induction generator based on the SVM Strategy," *Elektrotehniški Vestnik*, Vol. 84, No. 5, pp. 235–240, 2017.

[23] H. Benbouhenni, Z. Boudjema, and A. Belaidi, "Sensorless twelve sectors implementation of neural DPC controlled DFIG for reactive and active powers ripples reduction," *Majlesi Journal of Energy Management*, Vol. 7, No. 2, pp. 13–21, 2018.

[24] H. Benbouhenni, "A new SVM scheme based on ANN controller of a PMSG controlled by DPC strategy," *Majlesi Journal of Energy Management*, Vol. 7, No. 1, pp. 11–19, 2018.

[25] H. Benbouhenni, "A direct power control of the doubly fed induction generator based on the three-level NSVPWM technique," *International Journal of Smart Grid*, Vol. 3, No. 4, pp. 216–225, 2019.

[26] H. Benbouhenni, "Application of five-level NPC inverter in DPC-ANN of doubly fed induction generator for wind power generation systems," *International Journal of Smart Grid*, Vol. 3, No. 3, pp. 128–137, 2019.

[27] H. Benbouhenni, "Direct power control of a DFIG fed by a seven-level inverter using SVM strategy," *International Journal of Smart Grid*, Vol. 3, No. 2, pp. 54–62, 2019.

[28] H. Benbouhenni, "Stator current and rotor flux ripples reduction of DTC DFIG drive using FSTSMC algorithm," *International Journal of Smart Grid*, Vol. 3, No. 4, pp. 226–234, 2019.

[29] H. Benbouhenni, Z. Boudjema, and A. Belaidi, "Higher control scheme using neural second order sliding mode and ANFIS-SVM strategy for a DFIG-based wind turbine," *International Journal of Advances in Telecommunications, Electrotechnics, Signals and Systems*, Vol. 8, No. 2, pp. 17–28, 2019.

[30] H. Benbouhenni, Z. Boudjema, and A. Belaidi "Using three-level fuzzy space vector modulation method to improve indirect vector control strategy of a DFIG based wind energy conversion systems," *International Journal of Smart Grid*, Vol. 2, No. 3, pp. 155–171, 2018.

[31] S. Massoum, A. Meroufel, B. E. Youcefa, A. Massoum, and P. Wira, "Three-level NPC Converter-based Neuronal Direct Active and Reactive Power Control of the Doubly fed Induction Machine for Wind Energy Generation," *Majlesi Journal of Electrical Engineering*, Vol. 11, No. 3, pp. 25–32, 2017.

[32] M. V. Kazemi, A. S. Yazdankhah, and H. M. Kojabadi, "Direct power control of DFIG based on discrete space vector modulation," *Renewable Energy*, Vol. 35, pp. 1033-1042, 2010.

[33] S. Beneleghali, M. E. H. Benbouzid, J. F. Charpentier, T. Ahmed-Ali, and I. Munteanu, "Experimental validation of a marine current turbine simulator: Application to a PMSG-based system second-order sliding mode control," *IEEE Transactions on Industrial Electronics*, Vol. 58, pp. 118–126, 2011.

[34] H. Benbouhenni, Z. Boudjema, and A. Belaidi, "DPC based on ANFIS super-twisting sliding mode algorithm of a doubly-fed induction generator for wind energy system," *Journal Européen des Systèmes Automatisés*, Vol. 53, No. 1, pp. 69–80, 2020.

[35] C. Lascu and F. Blaabjerg, "Super-twisting sliding mode direct torque control of induction machine drives," in *IEEE Energy Conversion Congress and Exposition*, Pittsburgh, PA, pp. 5116–5122, Sep. 2014.

[36] H. Benbouhenni, "Intelligence indirect vector control of a DFIG based wind turbines," *Majlesi Journal of Electrical Engineering*, Vol. 13, No. 3, pp. 27–35, 2019.

H. Benbouhenni was born in chlef, Algeria. He is a Ph.D. student in the Departement of Electrical Engineering at the ENPO-MA, Oran, Algeria. He received a M.A. degree in Automatic and Informatique Industrial in 2017. His research activities include the application of robust control in the wind turbine power systems.

Z. Boudjema was born in Algeria in 1983. He is Teacher in University of Chlef, Algeria. He received a M.Sc. degree in Electrical Engineering from ENP of Oran, Algeria in 2010. He received a Ph.D. in Electrical Engineering from University of Sidi Belabes, Algeria 2015. His research activities include the study and application of robust control in the wind-solar power systems.

A. Belaidi is a Professor at the National Polytechnic High School - Maurice Audin in Oran. He obtained his Ph.D. in Physics at the University Of East Anglia - UK in 1980. His current fields of interest are nanotechnology, robotics, and artificial intelligence.